Journal of Fluids and Structures 17 (2003) 887–901

JOURNAL OF FLUIDS AND STRUCTURES

www.elsevier.nl/locate/jnlabr/yjfls

Perturbed interaction between vortex shedding and induced vibration

L. Cheng*, Y. Zhou, M.M. Zhang

Department of Mechanical Engineering, The Hong Kong Polytechnic University, Hung Hom, Kowloon, Hong Kong

Received 25 March 2002; accepted 3 March 2003

Abstract

This paper presents a novel technique to perturb interactions between vortex shedding from a bluff body and vortex-induced vibration of the body, with a view to provide a possible control of both flow and structural vibration. The essence of the technique is to create a local perturbation on the surface of a bluff body using piezoelectric ceramic actuators. Experiments were carried out in a wind tunnel. A square cylinder of height h, flexibly supported on springs at both ends, was allowed to vibrate only in the lift direction. Three actuators were embedded underneath one side, parallel to the flow, of the cylinder. They were simultaneously activated by a sinusoidal wave, thus causing the cylinder surface to oscillate. The structural displacement Y and flow velocity u were simultaneously measured using a laser vibrometer and a single hot wire, respectively. When the normalized vortex shedding frequency f_s^* synchronized with the natural frequency, f_n', of the dynamic system, Y was estimated to be about $0.08h$. This displacement collapsed to 25% once the actuators were excited at a normalized perturbation frequency of $f_p^* = 0.1$ and amplitude of $0.028h$. Flow visualization captured drastically impaired vortices shed from the cylinder. Spectral analysis of the Y and u signals points to the fact that the perturbation has altered the spectral phase ϕ_{Yu} at f_s between fluid excitation and structural vibration from 0 to π, and meanwhile decreased the spectral coherence Coh_{Yu} at f_s from 0.65 to 0.15. However, as f_p^* falls within the possible synchronization range ($f_p^* = 0.11-0.26$ or $0.8f_n' \sim 2f_n'$) where $f_n' = f_s$, ϕ_{Yu} at f_s remains near 0, the maximum Coh_{Yu} even reaching 0.9. As a result, both vortex shedding and the structural vibration are enhanced. It is expected that the perturbation technique presently investigated will have an important role to play in the flow-induced vibration control, especially with the active control element assimilated into the system.

1. Introduction

When a two-dimensional bluff body is subject to a cross-flow, vortex shedding from the structure creates fluid excitation forces, which in turn causes the structure to vibrate. The resultant structural motion influences the flow field, giving rise to fluid–structure coupling and modifying the frequency and magnitude of the excitation forces. This type of fluid–structure interactions is widely seen in engineering and could have significant impact on the fatigue life of structures, even leading to disastrous consequences. Therefore, interest in understanding the associated physics and controlling the structural vibration is rapidly growing.

Previous passive methods frequently rely on adding surface protrusions, shrouds or near-wake stabilizers to the structures to modify vortex shedding (Zdravkovich, 1981). The methods have proved successful particularly in offshore explorations and marine hydraulics (Unal and Rockwell, 1987; Wilson and Tinsley, 1989). An active control system uses actuators driven by external energy sources through an electronic system called controller. Such a system

*Corresponding author. Tel.: +852-2766-6769; fax: +852-2365-4703.
E-mail address: mmlcheng@polyu.edu.hk (L. Cheng).

0889-9746/03/$ - see front matter
doi:10.1016/S0889-9746(03)00042-2

essentially involves the generation of additional action to alter the system dynamics or parameters such as damping and stiffness. The resulting control action will counteract the effect of the initial disturbance. Provided that controllers are properly designed, the performance of such systems strongly depends on the actuation mechanism. One of the key points to ensure a successful control is that actuators used should create significant effects on physical parameters to be controlled. This is the problem of controllability, which is one of the most crucial issues to be addressed in designing a control system. In the present case, a possible actuation mechanism should warrant significant effects on vortex shedding and the wake structure.

One of the strategies reported in the literature aimed at directly controlling the structural vibration. Berger (1967) was probably the first to introduce the concept of feedback control to suppress wake instability. He used a feedback signal from a hot wire placed in the wake to actuate a bimorph cylinder and reported the possibility to prevent vortex shedding at a low Reynolds number $\mathrm{Re} \equiv U_\infty h/\nu = 80$, where U_∞ is the free-stream velocity, h is the characteristic height of the cylinder, and ν is the kinematic viscosity. Warui and Fujisawa (1996) used a similar feedback system to directly control a circular cylinder vibration at a moderate Reynolds number of 6700. In their study, electromagnetic actuators were installed at both ends of the cylinder to create an oscillation in the lateral direction. Their hot-wire measurements and flow visualization indicated weakening vortex strength. Baz and Ro (1991) used an electromagnetic actuator installed inside a cylinder to exert a force on the cylinder. The actuator was driven by a feedback flow velocity signal measured using a hot wire, thus increasing damping to the cylinder and effectively reducing the vortex-induced vibration at the occurrence of resonance, when the vortex shedding frequency, f_s, coincided with the natural frequency, f_n', of the system. Bonding piezoceramic actuators (PZT) on a plate surface to excite the structure, Caillaud et al. (2000) attempted to actively alter the damping of a flexible tube bundle in a cross-flow using velocity feedback to derive critical velocities, at which fluidelastic instabilities occur.

An attempt has been made to employ acoustic signals to control the flow field. Ffowcs-Williams and Zhao (1989) used a hot-wire signal to provide a feedback into a loudspeaker mounted on the wind tunnel wall. The acoustic excitation from the loudspeaker suppressed vortex shedding from a cylinder ($\mathrm{Re} = 400$). Roussopoulos (1993) revisited the problem, and concluded that the onset Reynolds number for vortex shedding could be increased by 20% as a result of the control.

In the aforementioned work, control was exerted to either the entire fluid field or cylinder, which may be roughly referred to as *global control*. A different approach is to perturb flow locally, and perhaps this may be classified as *local control*. Lewit (1992) used a feedback hot-wire signal to activate sound waves inside a circular tube. The sound waves interacted with flow through two rows of holes, located $\pm 90^\circ$ away from the forward stagnation line of the tube, respectively. The sound waves from the two rows of holes were in anti-phase, thus suppressing vortex shedding from the tube up to $\mathrm{Re} = 10^4$. Huang (1996) introduced the sound, again generated inside a cylinder and activated by a feedback hot-wire signal from the wake, into flow through a thin slit on the cylinder surface. He found that the shear flow around the slit could be modified so that vortex shedding could be suppressed up to a Re range between 4×10^3 and 1.3×10^4. Both investigations applied a high level of acoustic excitation (more than 120 dB) in order to produce sufficient control effects. This may not be a feasible solution in situations where noise is also a concern.

In contrast to closed-loop active control, which always makes use of a feedback signal from vortex shedding, a disturbance that does not have apparent relationship to vortex shedding has also been demonstrated to be effective in flow control. Williams et al. (1992) investigated the effect of symmetric and antisymmetric perturbation on the flow field at a frequency of $1.8f_s$. The perturbation was created by ejecting and sucking water through two rows of holes, located $\pm 45^\circ$ away from the forward stagnation line of the cylinder, respectively, into a water flow ($\mathrm{Re} = 470$). He observed a modified f_s and flow structure. Using acoustic waves emitted from a slot on the surface of a cylinder, Hsiao and Shyu (1991) demonstrated that a local perturbation near the shear-layer instability frequency and around the flow separation point caused an increase in lift and a reduction in drag and the scale of vortices. In both investigations, the cylinder was rigid, fix-supported at both ends. Therefore, no information was provided on the perturbation effect on interactions between vortex shedding and induced structural vibration. Furthermore, a very high perturbation frequency, compared with f_s, was used. It remains to be seen how vortex shedding and induced vibration would be affected by the perturbation of a frequency lower than f_s, which is difficult to implement in acoustic perturbations.

The present work proposes an alternative to the existing local control. A novel technique based on piezoelectric ceramic actuators is developed to alter vortex shedding and hence control vortex-induced structural vibration. The essence of the technique is to create a local perturbation on the surface of bluff bodies using piezoelectric ceramic actuators. When placed within an electric field, the piezoelectric effect results in a strain in the material. Piezoelectric ceramic material is characterized by its being lightweight and its capability of generating large forces over a wide range of frequencies. Conventional piezoelectric wafers can only generate very small deformation, which is probably why they have not been widely used in flow-induced vibration problems. The actuator presently investigated overcomes this obstacle by embedding a piezoelectric ceramic layer on the surface of a curved metallic thin plate. Due to its special

fabrication process and the effect of curvature, a relatively large displacement can be achieved, making it a potentially ideal candidate for flow-induced vibration control. When embedded in a vibrating structure, it is less intrusive and less bulky than most of the actuators such as loudspeakers and electromagnetic actuators. In addition, its operation, unlike acoustic actuators, does not generate any noise.

2. Experimental details

2.1. Actuators and their installation

The presently used piezoelectric ceramic actuators, called the THin layer composite UNimorph piezoelectric Driver and sEnsoR (THUNDER), were developed by the NASA Langley Research Center. To our knowledge, this actuator has so far been used for vibration isolation (Marouzé and Cheng, 2002), aeroelastic response control and airfoil shaping (Pinkerton and Moses, 1997). This type of actuators owes its large displacement range and load capacity to a particular fabrication process (Copeland et al., 1999). An ultrahigh performance hot-melt adhesive, LaRC™-SI, is used to bond metal foils to PZT ceramic at an elevated temperature, in order to create a pre-stressed condition when cooled to room temperature. A number of layers, whose coefficients of thermal expansion are different, are bonded, making up the composite laminate and giving the actuator special characteristics. As illustrated in Fig. 1, under an applied voltage, the actuator deforms out of plane, and is thus likely to generate much larger displacement than other piezoelectric ceramic actuators. Typically, without any loading, the actuator used in this paper may vibrate at a maximum displacement of about 2 mm and a frequency up to 2 kHz.

Note that the physics associated with vortex-induced vibrations on a bluff body in a cross-flow is in essence the same, irrespective of the cross-sectional shape of the bluff body, implying that a control technique applicable for one bluff body, say a circular cylinder, should be workable for another, such as a square cylinder, or vice versa. A square cylinder of height $h = 0.0152$ m made of aluminum alloy was presently selected as the test model because of ease in embedding actuators. A suitable installation of the actuators is crucial for obtaining a good performance. Various tests were conducted to find out the best way to install THUNDER actuators. Three actuators were embedded in series in a slot on one side of the cylinder (Fig. 2a,b) to support a thin plastic plate of 3 mm thick, which was installed flush with the cylinder surface. The length of the plastic plate is 493 mm, $\frac{2}{3}$ of the cylinder length. One end of each actuator was glue-fixed on the bottom side of the slot, while the other is free. The actuators and the walls of the slot around the actuators were well lubricated to reduce contact friction. To minimize the asymmetry of the dynamic system, the opposite side of the cylinder was identically constructed. Driven by the actuators, this plate will oscillate, reaching a 0.42 mm amplitude, or $0.028h$ under the resonance condition, to create the local perturbation of the cylinder surface. The root mean square (r.m.s.) displacement (not shown), measured using the laser vibrometer, is the same at different spanwise locations along the cylinder, suggesting a uniform oscillation of the surface. Furthermore, the movement of the surface in the streamwise or spanwise direction is essentially negligible. Thus, the perturbation is unlikely to cause any significant three-dimensionality of the flow.

The actuator is a dynamically nonlinear component. Its dynamic response may vary with the activating frequency, even though the imposed voltage is maintained at a constant. A test was conducted under no-flow conditions and a constant voltage on the actuators. The cylinder was fix-supported at both ends and could be approximately considered to be rigid as a whole. The deformation of the activated actuators causes a displacement Y_p on the plastic plate.

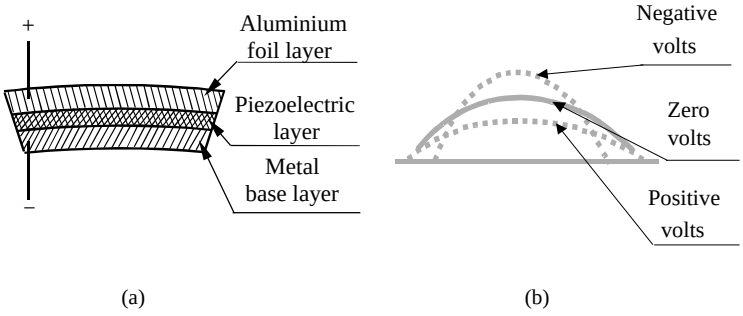

Fig. 1. Description of THUNDER actuators: (a) cross-sectional view; (b) typical deformation versus applied voltage.

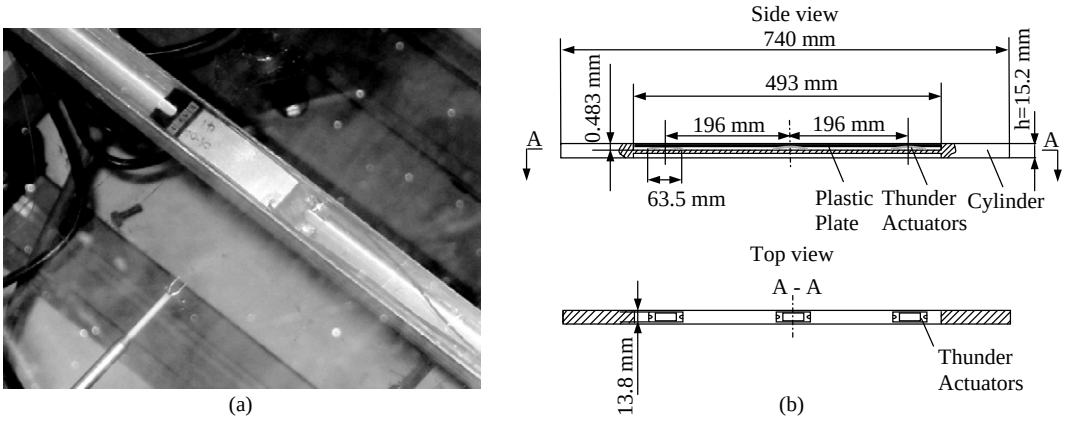

Fig. 2. Photograph (a) and schematic arrangement (b) of THUNDERs installed in the square cylinder.

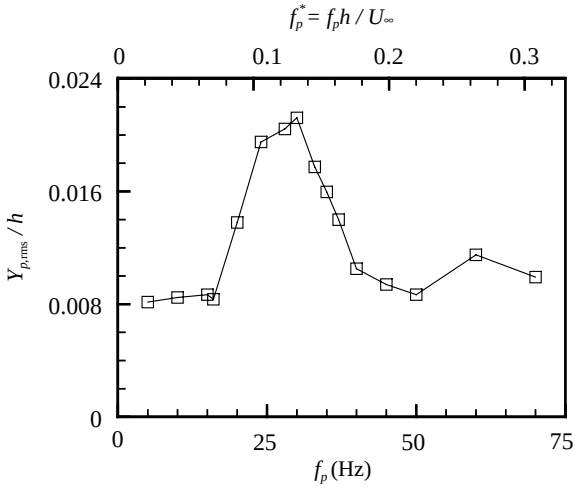

Fig. 3. Dependence of the perturbation amplitude on the perturbation frequency under a constant voltage (no flow).

The r.m.s. value $Y_{p,\mathrm{r.m.s.}}$ varies with the perturbation frequency f_p (Fig. 3), showing a maximum of $0.02h$. The actuators have been designed such that the peak in $Y_{p,\mathrm{r.m.s.}}$ occurs around the natural frequency, 30 Hz, of the cylinder system.

2.2. Experimental set-up

Experiments were carried out in a closed circuit wind tunnel with a square working section (0.6 m × 0.6 m) of 2.4 m in length. The wind speed of the working section is up to 50 m/s. The turbulent level is less than 0.4%. More details of the tunnel were given in Zhou et al. (2002). The experimental set-up is shown schematically in Fig. 4. The square cylinder, located at 0.2 m downstream of the exit plane of the contraction, spanned the full width of the working section. The cylinder was normal to the free-stream velocity, resulting in a blockage of about 2.5%. The cylinder upper surface would oscillate when the actuators were activated. The activating signal was generated by a signal generator and amplified by a dual-channel piezo driver amplifier (Trek PZD 700). The cylinder, flexibly supported on springs at both ends, was allowed to vibrate laterally.

The structural displacement, Y, and streamwise flow velocity, u, were measured simultaneously using a Polytec Series 3000 Dual Beam Laser Vibrometer (Zhou et al., 1999) and a 5 μm tungsten hot wire. The constant temperature circuit

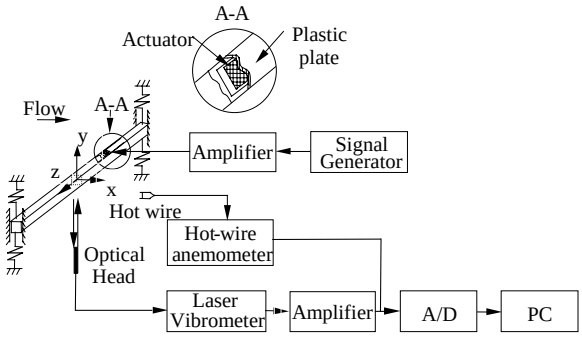

Fig. 4. Experimental set-up.

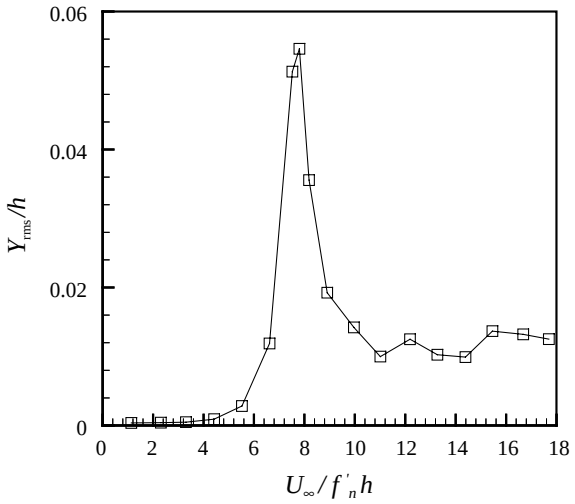

Fig. 5. The r.m.s. displacement, $Y_{\text{r.m.s.}}/h$, of the cylinder versus the reduced velocity, $U_r = U_\infty / f_n' h$.

was used for the operation of the hot wire at an overheat ratio of 1.8. The experimental uncertainty of the displacement measurement by laser vibrometer is estimated to be 0.5%. Signals from both the laser vibrometer and the hot wire were conditioned and digitized using a 12-bit A/D board at a sampling frequency of 3.5 kHz per channel. The duration of each record was about 20 s.

Using the half-power technique, the structural damping ratio, ζ, was estimated to be 1.71×10^{-3}, giving a reduced damping or Scruton number, $2m(2\pi\zeta)/\rho h^2$, of 15.2 in the synchronization range, where m is the mass per unit length of cylinder, ζ the damping factor and ρ the air density. The Scruton number is a very important parameter, which governs the synchronization between vortex shedding and induced vibration. This number is in this case well below the critical value, i.e. 64, as proposed by Blevins (1990), implying an oscillation of significant amplitude. The normalized r.m.s. value, $Y_{r.m.s.}/h$, of Y versus the reduced velocity U_r ($U_\infty / f_n' h$) is given in Fig. 5. $Y_{\text{r.m.s.}}/h$ shows its maximum, about 0.055, at $U_r \approx 7.8$ (Re = 3500), where the resonance occurs. The corresponding maximum displacement of the cylinder was about 1.2 mm, or $0.08h$. The correspondence between the measured Y/h and the Scruton number at resonance is in good agreement with the data given in Figs. 3 to 21 of Blevins (1990).

In order to visualize the perturbation effect on the flow structure, the laser-induced fluorescence (LIF) used was generated by means of the flow visualization function of a 3-D DANTEC particle image velocimetry (PIV) system. Flow was seeded by the smoke, generated from paraffin oil, of a particle size of about 1 m in diameter. The flow illumination was provided with a light sheet, generated by a 120 mJ Newwave pulsed laser. A Dantec Double Image 700

CCD camera was used to capture single-exposed digital particle images (each of 1280×1024 pixels). The horizon image magnification was of the order of 0.12 mm/pixel. A wide-angle lens was used to enlarge the view field so that each image covered an area of approximately 165 mm × 125 mm in the flow field. The recording interval between a pair of successive images was 0.2 s. Experiments were carried out at the same conditions as the hot wire and laser vibrometer measurements.

3. Effect of perturbation amplitude and frequency

Tests were conducted to document the effect of Y_p and f_p on the resonance. Fig. 6 presents the variation of the r.m.s. displacement, $Y_{\text{r.m.s.}}$, of the cylinder and the r.m.s. streamwise velocity, $u_{\text{r.m.s.}}$, with f_p. A constant voltage, whose r.m.s. value was 141 V, was applied on the actuators as f_p varied. The broken lines indicate $Y_{\text{r.m.s.}}$ and $u_{\text{r.m.s.}}$ without perturbation. $Y_{\text{r.m.s.}}$ and $u_{\text{r.m.s.}}$ exhibit similar variation with f_p. The maximum attenuation occurs at $f_p^* = f_p h/U_\infty = 0.1$, resulting in $Y_{\text{r.m.s.}} = 0.014h$ and $u_{\text{r.m.s.}} = 0.012U_\infty$. Unless otherwise stated, the asterisk in this paper denotes normalization by h and U_∞. For $f_p^* < 0.1$, both $Y_{\text{r.m.s.}}$ and $u_{\text{r.m.s.}}$ are smaller than those without perturbation, but appreciably larger than those at $f_p^* = 0.1$. It is worthwhile recalling that $Y_{p,\text{r.m.s.}}$ displays a broad peak between $f_p^* = 0.1$ and 0.13, and reduces substantially for $f_p^* < 0.1$ or $f_p^* > 0.13$ (Fig. 3). The variation in $Y_{p,\text{r.m.s.}}$ will have an impact on $Y_{\text{r.m.s.}}$. Fig. 7 shows the variation in $Y_{\text{r.m.s.}}$ with voltage, imposed on the actuators, at a fixed f_p^* (= 0.1). The voltage and $Y_{p,\text{r.m.s.}}$ are correlated, though not linearly (Wise, 1998). As the r.m.s. voltage increases from 0 to 141 V, $Y_{p,\text{r.m.s.}}$ should increase and hence $Y_{\text{r.m.s.}}$ decreases from $0.056h$ to $0.014h$. Therefore, the small $Y_{p,\text{r.m.s.}}$ for $f_p^* < 0.08$, as compared with that at $f_p^* = 0.1$ (Fig. 3), may partially account for the less effective attenuation in $Y_{\text{r.m.s.}}$ and also $u_{\text{r.m.s.}}$ (Fig. 6).

A pronounced peak in $Y_{\text{r.m.s.}}$ and $u_{\text{r.m.s.}}$ occurs at $f_p^* = 0.13$, coinciding with the frequency of vortex shedding from a square cylinder (e.g., Vickery, 1966; Lyn and Rodi, 1994; Zhou and Antonia, 1995), namely, $f_p^* = f_s^* = f_n'^*$. Both $Y_{\text{r.m.s.}}$ and $u_{\text{r.m.s.}}$ are doubled, compared with the unperturbed one. Apparently, perturbation leads to a much more violent resonance, acting as an 'amplifier'. As $f_p^* > f_s^* = f_n'^*$, the resonance is less 'amplified', but in general more violent than that without perturbation. Again, the decreased perturbation amplitude for $f_p^* > 0.13$ may be partially responsible for the less effective amplification than at $f_p^* = 0.13$.

Note that both $Y_{\text{r.m.s.}}$ and $u_{\text{r.m.s.}}$ exhibit local peaks at $f^* = 0.065$ and 0.26, namely at the sub-harmonic and the second harmonic of $f_n'^* = 0.13$. This is probably due to a partial synchronization between f_p^* and $f_n'^*$. The observation suggests that, in order to avoid violent resonance, perturbation should be avoided at a sub-harmonic or harmonic frequencies of the system's natural frequency.

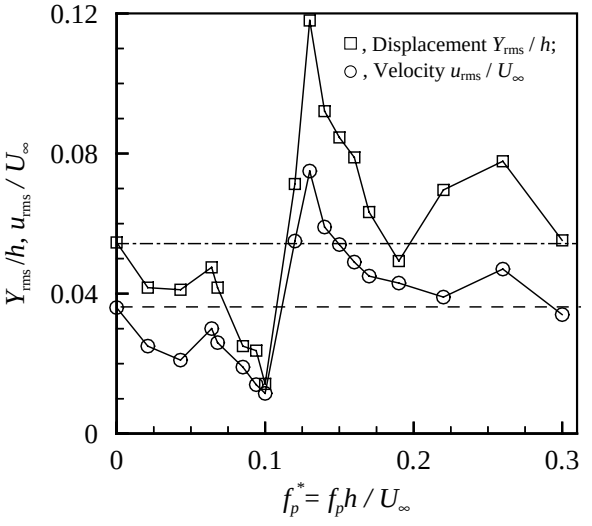

Fig. 6. The effect of the perturbation frequency on the cylinder displacement and the flow velocity (a constant voltage was applied). The broken lines indicate the level without perturbation. The hot wire was located at $x/h = 2$, $y/h = 1.5$.

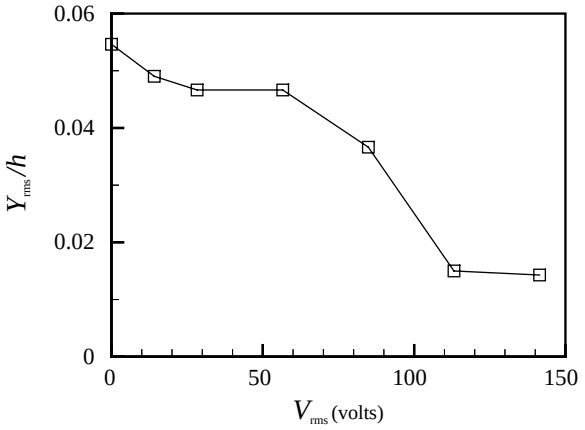

Fig. 7. Variation of the cylinder displacement with voltage applied on actuators.

4. Perturbation effect on fluid–structure interactions

In order to understand the perturbation effect on the fluid–structure interactions, the synchronizing flow excitation and structural vibration were perturbed at $f_p^* = 0.1$ and $Y_{p,\text{r.m.s.}} = 0.02h$ (measured without the flow). The results are examined and compared with those without perturbation. Before the cylinder was perturbed, its vibration amplitude Y along the lift direction was 1.2 mm or $0.08h$.

Fig. 8 shows the typical time histories of the perturbed and unperturbed signal Y. There is a drastic change; Y drops from a maximum of $0.08h$ in the absence of the perturbation to about $0.02h$ after being perturbed, about 75% attenuation. Furthermore, the perturbed signal is significantly less periodical than that without perturbation. The corresponding Y spectrum, E_Y (Fig. 9) displays a pronounced peak at $f_s^* = 0.13$ without perturbation. The spectrum of fluctuation α (α represents either Y or u) has been normalized so that $\int_0^\infty E_\alpha(f)\,\mathrm{d}f = 1$. The peak amplitude falls off from 0.625 to 0.129 because of perturbation; the attenuation percentage is consistent with the observation from the Y signal. Note that an additional peak at an amplitude of 0.0816 occurs at $f^* = 0.1$ in the perturbed E_Y, apparently due to perturbation.

A similar observation is made of the u signal. The fluctuating velocity amplitude was reduced due to perturbation by about 68% (Fig. 10); the peak amplitude in the perturbed E_u (Fig. 11) experiences an attenuation of 81%, suggesting a substantial decline in the strength of shedding vortices. Note that the spectra have been normalized so that $\int_0^\infty E_\alpha(f)\,\mathrm{d}f = 1$. The peak at $f^* = 0.13$ in E_u (Fig. 11b) was substantially weakened due to the perturbation ($f_p^* = 0.1$), compared with the unperturbed condition (Fig. 11a). As a result, energy at other frequencies increases relatively to the total energy. This appears more evident for $f_p^* < 0.12$. The peak at $f^* = 0.13$ in E_Y was also weakened due to the perturbation. But E_Y displays one additional peak at $f_p^* = 0.1$. The integration of E_Y over $f^* = 0.06$ to 0.2 (covering both peaks) indicates an increase, from 1.2×10^{-3} to 1.6×10^{-3}, in energy. Consequently, energy in other frequencies decreases, which again is more evident in lower frequencies.

The results in Figs. 8–11 are indeed corroborated by typical flow structures (Fig. 12) from flow visualization. The unperturbed shedding vortices (Fig. 12a) display a Kármán vortex street. However, when perturbation is present, the Kármán street is not so evident. The vortices (Fig. 12b) appear broken up, showing considerably less coherence and weaker strength than those unperturbed. Correspondingly, the cross-flow distribution of the mean velocity, $\bar{U}$, perturbed at $f_p^* = 0.1$ (Fig. 13) measured at $x/h = 3$ is quite different from that of the unperturbed case. The velocity defect is increased substantially, probably because the impaired vortices entrain less fluid of high speed from the free stream (Warui and Fujisawa, 1996).

In order to improve our understanding of the physics behind weakening vortex shedding and structural vibration, the simultaneously measured transient Y and u signals, while being perturbed, are examined in Fig. 14. Evidently, before perturbation is introduced, the two signals are synchronized because of the occurrence of the resonance. Once perturbed, at about 0.08 s, as indicated by one vertical broken line, the signals experience a rather short transition, taking about 0.03 s before settling down to a stable state. Then, the Y and u signals display not only reduced amplitude, but also a phase shift at the dominant frequency between them.

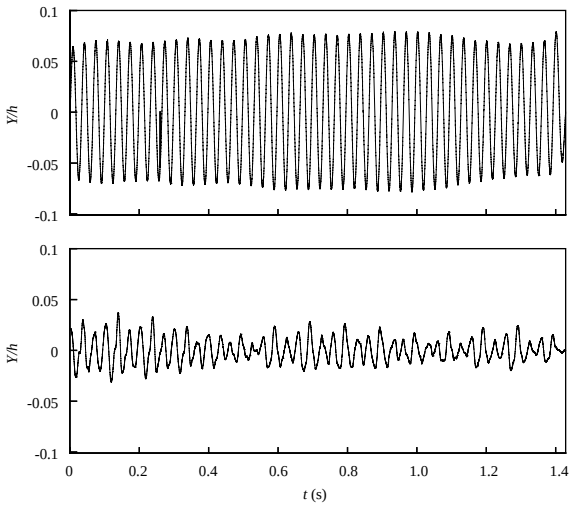

Fig. 8. Typical time histories of the cylinder displacement Y with (lower trace) and without (upper trace) perturbation. The time origin is arbitrary.

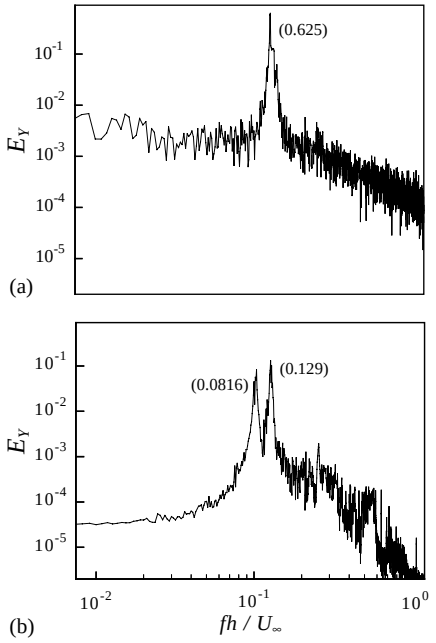

Fig. 9. Power spectrum of the displacement signal Y: (a) unperturbed, (b) perturbed.

The shift in phase between the two perturbed signals may be quantified by the spectral phase angle, defined by $\phi_{Yu}(\equiv \tan^{-1}(Q_{Yu}/Co_{Yu}))$. Co_{Yu} and Q_{Yu} are the cospectrum and quadrature spectrum of Y and u, respectively. Here, the cross-spectrum is computed from the Fourier transform of the correlation $\overline{Y(t+\tau)u(t)}$. See Zhang et al. (2000) for more details. Before perturbation, the spectral phase angle ϕ_{Yu} (Fig. 15a) shows a zero phase at $f_s^* = 0.13$, indicating synchronization between the Y and u signals. The plateau about $f_s^* = 0.13$ indicates synchronization between the two signals over a range of frequencies about f_s^*. The corresponding spectral coherence Coh_{Yu} (Fig. 16a) exhibits a peak at $f_s^* = 0.13$, amounting to 0.65. The spectral coherence between Y and u, defined by $Coh_{Yu} = (Co_{Yu}^2 + Q_{Yu}^2)/E_Y E_u$, provides a measure of the degree of correlation between the Fourier components of Y and u.

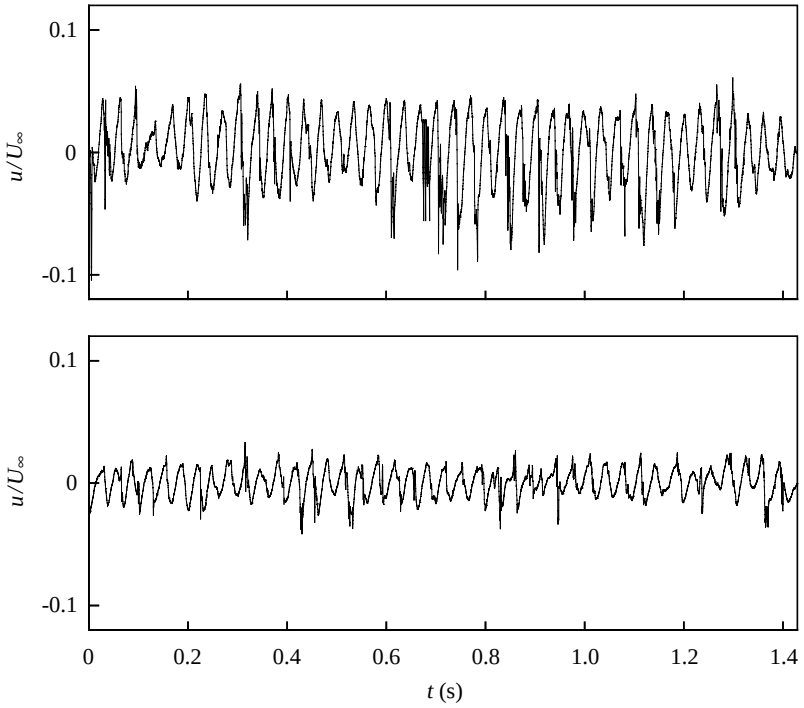

Fig. 10. Typical time histories of the streamwise flow velocity u with (lower trace) and without (upper trace) perturbation. The time origin is arbitrary. The hot wire was located at $x/h = 2$, $y/h = 1.5$.

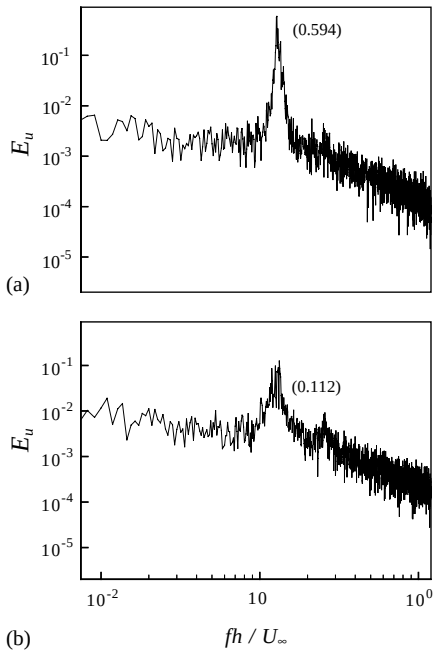

Fig. 11. Power spectrum of the hot-wire signal u: (a) unperturbed, (b) perturbed. The hot wire was located at $x/h = 2$, $y/h = 1.5$.

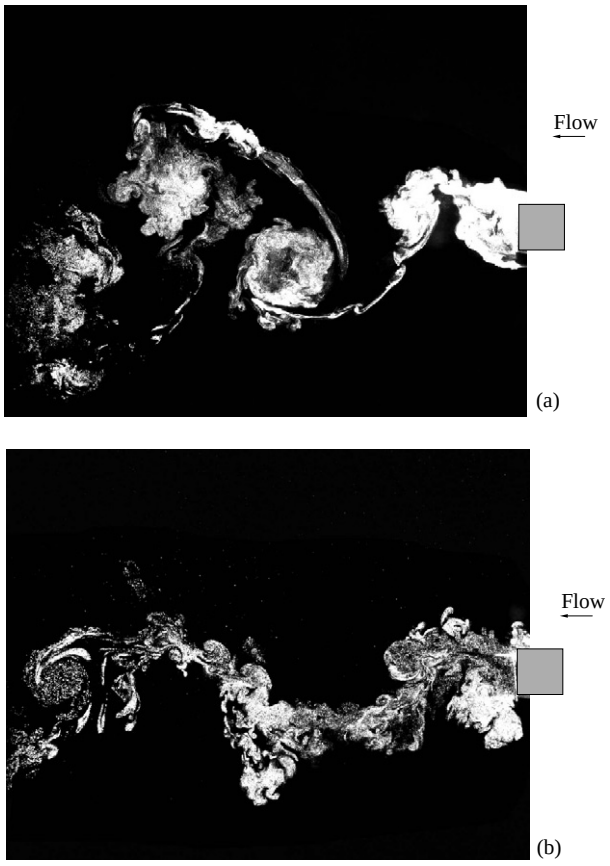

Fig. 12. Typical flow structure: (a) unperturbed, (b) perturbed.

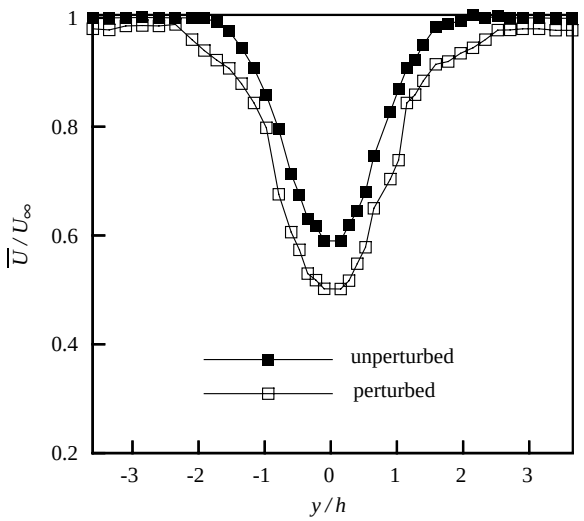

Fig. 13. Cross-flow distribution of mean velocity with and without perturbation at $x/h = 3$. The perturbation frequency (f_p^*) is 0.1 and the Reynolds number is 3500.

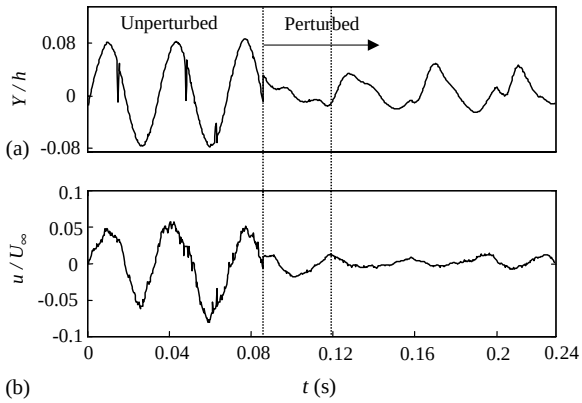

Fig. 14. Transition of displacement (a) and hot-wire (b) signals as actuators were activated. The time origin is arbitrary. The hot wire was located at $x/h = 2$, $y/h = 1.5$.

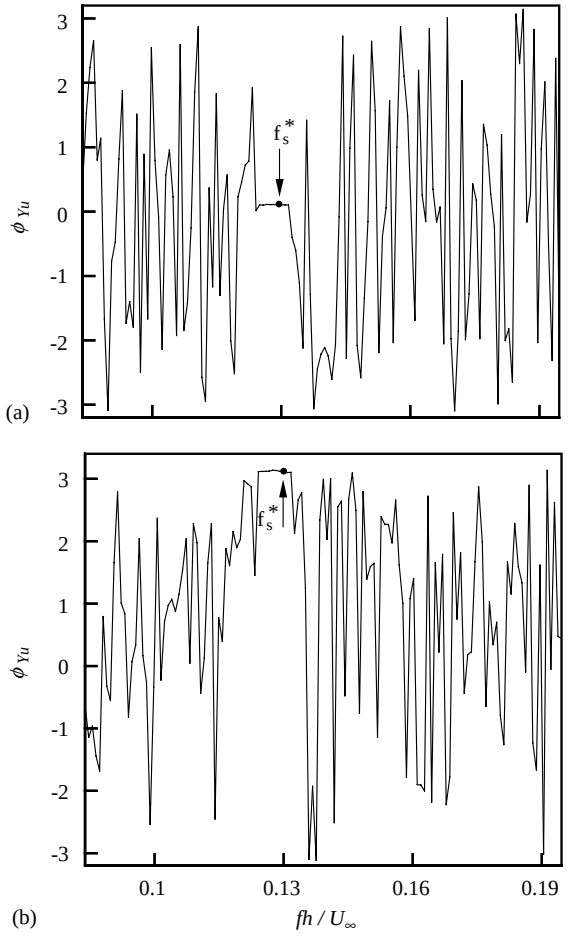

Fig. 15. The phase shift ϕ_{Yu} between the Y and u signals: (a) actuators were not activated; (b) actuators were activated. The hot wire was located at $x/h = 2$, $y/h = 1.5$.

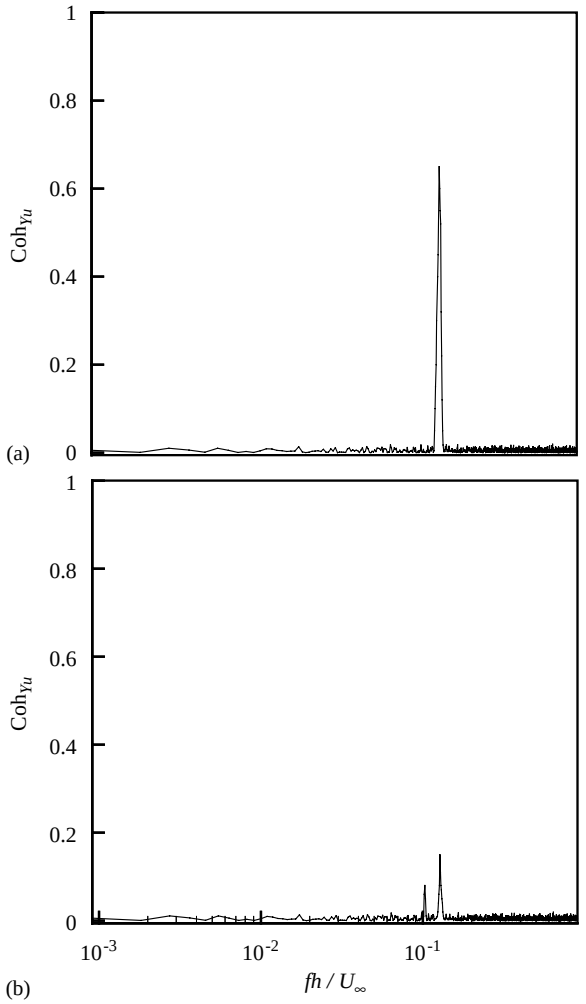

Fig. 16. Spectral coherence between the Y and u signals: (a) actuators were not activated; (b) actuators were activated. The hot wire was located at $x/h = 2$, $y/h = 1.5$.

Once perturbed, ϕ_{Yu} (Fig. 15b) shows a phase of π at $f_s^* = 0.13$, suggesting that structural vibration and vortex shedding are in anti-phase. Correspondingly, Coh_{Yu} (Fig. 16b) exhibits a tiny peak at $f_s^* = 0.13$, reaching only 0.15. In a turbulent near-wake, vortices are highly coherent. As a matter of fact, the phase lag at f_s between lateral velocity signals is approximately zero across the wake even at $x/d = 10$ (Zhou et al., 2002). Speculatively, the phase at f_s of the measured streamwise velocity, u, at $x/h = 2$ and $y/h = 1.5$ could be the same as that of u at $x/h = 0$ because of the strong coherence of the shear layer separating from the cylinder. Note that the lateral velocity component, v, leads u within the Karman vortex by about $\pi/2$ for $y/d > 0$ (Zhou and Antonia, 1993). This implies that the measured u could be about $\pi/2$ lagging behind that of v at $x/h = 0$. On the other hand, given that the cylinder oscillates harmonically, the measured Y is $\pi/2$ lagging behind the cylinder velocity $\dot{Y}$. Therefore, the phase relationship between u and Y could represent that between v and $\dot{Y}$. At zero phase, v and $\dot{Y}$ synchronize, re-enforcing each other. At the phase of π, v and $\dot{Y}$ are opposite in direction, implying that the flow and structural vibration now act against each other, thus resulting in the drastically reduced vibration amplitude (Figs. 8 and 10) and vortex strength (Figs. 9 and 11). A better understanding of the physics behind the observation perhaps requires the knowledge of the 3-D aspects of the flow, which are not measured presently.

It is pertinent to comment that the impaired cylinder vibration is unlikely owing to a forcing frequency detuned from the system's natural frequency. In principle, any change in flow–structure interactions could change the mass loading on

the structure, leading to a change in the natural frequencies of the system. However, the added mass is small in air-flow. A comparison between the power spectral density functions E_Y (Fig. 9) before and after the perturbation indicates no appreciable change of the natural frequency of the fluid–cylinder system (the uncertainty in the estimate of frequencies in spectral analysis is about 0.13 Hz). Even if the natural frequency changes slightly, it may still fall in the synchronization range of $U_r \approx 7 \sim 8.5$ (Fig. 5).

It has been shown in Section 3 that $Y_{\text{r.m.s.}}$ and $u_{\text{r.m.s.}}$ vary with f_p. The calculated ϕ_{Yu} at $f_s^* = 0.13$ (Fig. 17) shows that the Y and u signals tend to be in anti-phase for $f_p^* \leqslant 0.1$ but in phase for $f_p^* \geqslant 0.12$. Correspondingly, Coh_{Yu} (Fig. 18) is reduced for $f_p^* \leqslant 0.1$, showing a minimum at $f_p^* = 0.1$. For $f_p^* \geqslant 0.12$, Coh_{Yu} is enhanced, climbing to a maximum at $f_s^* = 0.13$. The results are internally consistent with those in Fig. 6. One can conclude that perturbation tends to break the phase 'lock-in' between vortex shedding and structural vibration for $f_p^* \leqslant 0.1$. Therefore, flow and structural motions

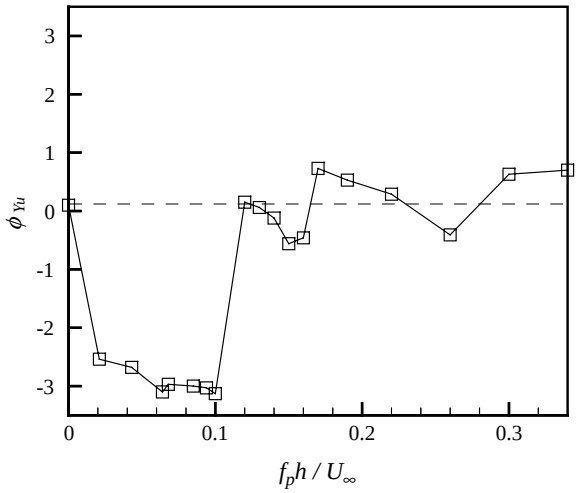

Fig. 17. The effect of the perturbation frequency on the phase shift ϕ_{Yu} at $f_s^* \approx 0.13$ between the Y and u signals. The hot wire was located at $x/h = 2$, $y/h = 1.5$.

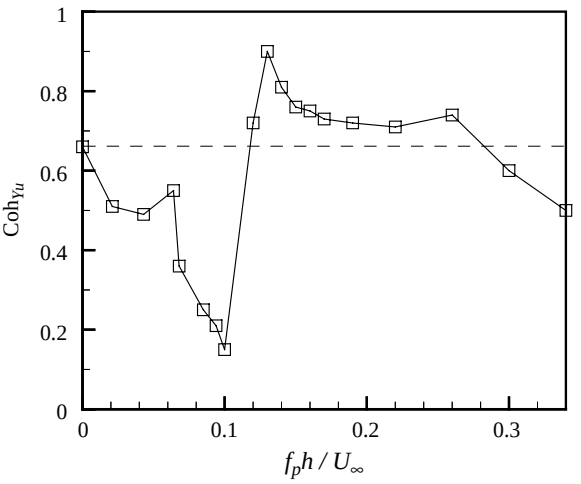

Fig. 18. The effect of the perturbation frequency on the spectral coherence at $f_s^* \approx 0.13$ between Y and u signals. The hot wire was located at $x/h = 2$, $y/h = 1.5$.

act against each other. On the other hand, the synchronization between vortex shedding and structural vibration is retained for $f_p^* \geqslant 0.12$, and as a matter of fact is further enhanced up to $f_p^* = 2f_s^*$.

Gowda (1975) found that, for bluff bodies with fixed separation points, the synchronization between vortex shedding and induced vibration began at $f_s \approx 0.8f_n'$ and ended when $f_s \approx 2f_n'$. This corresponds here to a frequency range of $f^* = 0.11-0.26$, coinciding with the range of enhanced resonance. It seems plausible that, as f_p^* falls within the possible synchronization range, it is difficult for perturbation to break the synchronization between vortex shedding and structural vibration; instead, the perturbation is more likely to increase the strength of synchronization or resonance. However, once f_p^* is outside the possible synchronization range, it is easy for perturbation to decouple the synchronization between vortex shedding and structural vibration, resulting in reduced $Y_{\text{r.m.s.}}$ and $u_{\text{r.m.s.}}$.

It is pertinent to comment that the range of frequencies, where perturbation amplitude is large (or perturbation is effective), is relatively small. But this does not imply that these actuators are not robust. Firstly, in engineering, violent vibration occurs mostly at the resonance, which is in general associated with a narrow band of frequencies, that is, an effective perturbation does not necessarily have to cover a wide band of frequencies. The frequency range (Fig. 3) of the actuators, where perturbation amplitude is large, exceeds that of resonance and is further adjustable to suit different needs. Secondly, once active control is introduced, the efficiency of the technique should be greatly enhanced, and the perturbation amplitude required to control vortex-induced vibrations can be substantially reduced.

5. Conclusions

A perturbation technique using piezoelectric ceramic actuators for flow-induced vibration control has been proposed. Being embedded in the structure, the actuators are less intrusive to flow and less bulky than many conventional actuators such as loudspeakers and electromagnet actuators. Activated by a sinusoidal wave, the actuators produce a periodic deformation on the cylinder surface, thus altering interactions between synchronizing cylinder motion and vortex shedding. Subsequently, both vortex shedding and flow-induced vibration are modified. The following conclusions can be drawn.

(i) The perturbation can be very effective in attenuating the violent resonance between vortex shedding and structural vibration. It has been observed that, with a perturbation at amplitude of $0.028h$, the maximum structural displacement at resonance was reduced from $0.08h$ to $0.02h$. Meanwhile, the vortices shed from the cylinder have been weakened drastically as indicated by both hot-wire (down to 19% in the u spectrum) and LIF measurements.

(ii) Interactions between vortex shedding and the structural vibration are sensitive to the perturbation frequency. As f_p^* falls within the possible synchronization range (0.11–0.26 or $0.8f_n' \sim 2f_n'$), where $f_n' = f_s$, perturbation could not break the bond in the synchronization between structural displacement and vortex shedding; rather it tends to reinforce the resonance. At $f_p^* = 0.13$, Coh_{Yu} climbs from 0.65 without perturbation to 0.9 with perturbation. Correspondingly, the resonance is the most violent, both $Y_{\text{r.m.s.}}$ and $u_{\text{r.m.s.}}$ being doubled. Two factors are probably responsible. First, at this f_p^*, f_n' is identical to the natural vortex shedding frequency; the resonance without perturbation is likely to be strong. Second, the perturbation amplitude is the largest (Fig. 3). However, when f_p^* is beyond the possible synchronization range, perturbation changes the phase relationship between synchronizing structural displacement and vortex shedding from zero to near π. Meanwhile, the spectral coherence Coh_{Yu} at f_s between the Y and u signals is reduced from 0.65 to 0.15, effectively attenuating the resonance. The maximum attenuation occurs at a perturbation frequency of $f^* = 0.1$, where the perturbation amplitude is very large.

The present investigation points to a great potential for the piezoelectric ceramic actuators for flow-induced vibration control, especially with the introduction of active control, which may ensure a desired relationship between structural vibration and vortex shedding. The present control technique may possibly be extended to other applications, e.g. the control of galloping instability and vortex-induced vibrations on the cylinders of other cross-sectional geometries.

Acknowledgements

The authors wish to acknowledge support given to them by the Central Research Grant of The Hong Kong Polytechnic University through Grant G-W108.

References

Baz, A., Ro, J., 1991. Active control of flow-induced vibrations of a flexible cylinder using direct velocity feedback. Journal of Sound and Vibration 146, 33–45.

Berger, E., 1967. Suppression of vortex shedding and turbulence behind oscillating cylinders. Physics of Fluids 10, 191–193.

Blevins, R.D., 1990. Flow-Induced Vibration. Krieger Publishing Company, Malabar, FL, p. 477.

Caillaud, S., de Langre, E., Piteau, P., 2000. Measurement of critical velocities for fluidelastic instability using vibration control. Journal of Vibration and Acoustics 122, 341–345.

Copeland, B.M., Buckley, J.D., Bryant, R.G., Fox, R.L., Hellbaum, R.F., 1999. THUNDER—an ultra-high displacement piezoelectric actuator. NASA Langley Research Center, Hampton, VA 23681-0001, USA.

Ffowcs-Williams, J.E., Zhao, B.C., 1989. The active control of vortex shedding. Journal of Fluids and Structures 3, 115–122.

Gowda, B.H.L., 1975. Some measurements on the phenomenon of vortex shedding and induced vibrations of circular cylinders. Deutsche Luft- und Raumfahrt Forschungsbericht, No. 75-01.

Hsiao, F.B., Shyu, J.Y., 1991. Influence of internal acoustic excitation upon flow passing a circular cylinder. Journal of Fluids and Structures 5, 427–442.

Huang, X.Y., 1996. Feedback control of vortex shedding from a circular cylinder. Experiments in Fluids 20, 218–224.

Lewit, M., 1992. Active control of dipole sound from cylinders. Proceedings of the DAGA'92, Berlin, Germany.

Lyn, D.A., Rodi, W., 1994. The flapping shear layer formed by flow separation from the forward corner of a square cylinder. Journal of Fluid Mechanics 267, 353–376.

Marouzé, J.P., Cheng, L., 2002. A feasibility study of active vibration isolation using THUNDER actuators. Smart Materials and Structures 11, 854–862.

Pinkerton, J.L., Moses, R.W., 1997. A feasibility study to control airfoil shape using THUNDER, NASA Technical Memorandum 4767.

Roussopoulos, K., 1993. Feedback control of vortex shedding at low Reynolds numbers. Journal of Fluid Mechanics 248, 267–296.

Unal, M.F., Rockwell, D., 1987. On vortex formation from a cylinder Part 2. Control by splitter–plate interference. Journal of Fluid Mechanics 190, 513–529.

Vickery, B.J., 1966. Fluctuating lift and drag on a long cylinder of square cross-section in a smooth and turbulent stream. Journal of Fluid Mechanics 25, 481–494.

Warui, H.M., Fujisawa, N., 1996. Feedback control of vortex shedding from a circular cylinder by cross-flow cylinder oscillations. Experiments in Fluids 21, 49–56.

Williams, D.R, Mansy, H., Amato, C., 1992. The response and symmetry properties of a cylindrical wake subjected to localized surface excitation. Journal of Fluid Mechanics 234, 71–96.

Wilson, J.F., Tinsely, J.C., 1989. Vortex load reduction: experiments in optimal helical strake geometry for rigid cylinders. ASME Journal of Energy Resources Technology 111, 72–76.

Wise, S.A., 1998. Displacement properties of RAINBOW and THUNDER piezoelectric actuators. Sensors and Actuators A 69, 33–38.

Zdravkovich, M.M., 1981. Review and classification of various aerodynamic and hydrodynamic means for suppressing vortex shedding. Journal of Wind Engineering and Industrial Aerodynamics 7, 145–189.

Zhang, H.J., Zhou, Y., Antonia, R.A., 2000. Longitudinal and spanwise structures in a turbulent wake. Physics of Fluids 12, 2954–2964.

Zhou, Y., Antonia, R.A., 1993. A study of turbulent vortices in the wake of a cylinder. Journal of Fluid Mechanics 253, 643–661.

Zhou, Y., Antonia, R.A., 1995. Memory effects in turbulent plane wakes. Experiments in Fluids 19, 112–120.

Zhou, Y., So, R.M.C., Jin, W., Xu, H.G., Chan, P.K.C., 1999. Dynamic strain measurements of a circular cylinder in a cross flow using a fiber Bragg grating sensor. Experiments in Fluids 27, 359–367.

Zhou, Y., Zhang, H.J., Liu, M.W., 2002. The turbulent wake of two side-by-side circular cylinders. Journal of Fluid Mechanics 458, 303–332.